New Journal of Physics
The open access journal at the forefront of physics

Deutsche Physikalische Gesellschaft DPG IOP Institute of Physics

Bending-induced diminution of shape resonances in the core-level absorption region of hot CO_2 and N_2O

To cite this article: T Tanaka *et al* 2010 *New J. Phys.* **12** 123017

New Journal of Physics
The open-access journal for physics

Bending-induced diminution of shape resonances in the core-level absorption region of hot CO_2 and N_2O

T Tanaka[1], M Hoshino[1], R R Lucchese[2], Y Tamenori[3], H Kato[1], H Tanaka[1] and K Ueda[4,5]

[1] Department of Physics, Sophia University, Tokyo 102-8554, Japan
[2] Department of Chemistry, Texas A&M University, College Station, TX 77843-3255, USA
[3] Japan Synchrotron Radiation Research Institute, Sayo-gun, Hyogo 679-5198, Japan
[4] Institute of Multidisciplinary Research for Advanced Materials, Tohoku University, Sendai 980-8577, Japan
E-mail: ueda@tagen.tohoku.ac.jp

New Journal of Physics **12** (2010) 123017 (18pp)
Received 19 May 2010
Published 9 December 2010
Online at http://www.njp.org/
doi:10.1088/1367-2630/12/12/123017

Abstract. We have measured the initial vibrational-state-specific, symmetry-resolved ion-yield spectra of CO_2 and N_2O in the shape resonance regions above the K-shell ionization thresholds. For both molecules, significant diminution of the shape resonances by bending excitation in the initial electronic ground state is observed. The measured ion-yield spectra are well reproduced by calculations employing the Schwinger variational principle. The observed changes in the spectra are seen to be due to a shift of the resonances to lower energy and an initial increase in width with bending.

[5] Author to whom any correspondence should be addressed.

Contents

1. Introduction 2
2. Experimental methods 3
3. Theoretical methods 4
4. Results and discussion 5
5. Conclusions 16
Acknowledgments 17
References 17

1. Introduction

Shape resonances are often prominent features of low-energy electron–molecule scattering and of photoionization with photoelectron energies less than about 50 eV [1]. A shape resonance is caused by the dynamical trapping of an electron in the vicinity of a molecule. The trapping is due to the effects of the generally attractive electron–molecule interaction potential and angular momentum, which can lead to an effective repulsive potential keeping the electron away from the molecule [2]. The combination of these two terms in the potential can lead to effective potential barriers through which a trapped photoelectron must tunnel to escape from the molecule. For simple diatomic systems, the only geometric parameter that can affect the position and width of a shape resonance is the bond length. In such systems, a simple particle-in-a-box model provides a qualitative understanding of the usual behavior of the resonant energy, i.e. the energy goes down as the bond is made longer. The widths of such resonances also typically go down as the energy becomes lower. The behavior of the resonance widths is understood as being due to the fact that for nonzero angular momentum, i.e. $l > 0$, the energy deficit between the energy of the photoelectron and the top of the effective potential energy barrier becomes larger as the energy of the photoelectron approaches the threshold, leading to longer lifetimes and narrower resonance widths. In larger molecular systems, the connection between geometry changes and the position and width of a resonance is not always so simple. For example, in the photoionization of C_6F_6 the symmetric increase of the C–F bonds leads to a decrease in energy of a resonant state while at the same time increasing the width of the resonance [3].

In the present study, we consider the effects of bending vibrational excitation in the initial state on the photoionization process, and in particular we examine the effects on shape resonances. This study is of interest not only from the perspective of fundamental properties of shape resonances but also because such vibrationally excited molecules occur in nature. This is especially true in the ionosphere and in astrophysical circumstances. In spite of the large abundance and importance of these vibrational excited molecules, most experimental studies have dealt with room-temperature molecules in the vibrational ground state. To our knowledge, there are very few studies of high-temperature, vibrationally excited molecules in the areas of extreme vacuum ultraviolet absorption spectroscopy [4] and low-energy electron collisions ([5] and references therein; [6]).

If a molecule is vibrationally excited, the vibrational wave function has a larger spatial extent than that of the vibrational ground state. Thus, spectroscopic studies of vibrationally excited molecules can also probe different regions of potential surfaces of electronically excited

states. Furthermore, molecules in which non-totally symmetric vibrations are excited may exhibit new properties due to symmetry breaking. Indeed in previous work, owing to these two aspects, we have successfully probed dramatically enhanced vibronic coupling effects in the x-ray absorption spectra of the vibrational excited triatomic molecules [7]–[9].

In this paper, we demonstrate that the excitation of a bending vibration in the electronic ground state significantly affects the σ^* shape resonances of the x-ray absorption spectra. In the case of photoionization, it is well known that the shape resonance energies are sensitive to the final ionic vibrational state because the shape resonance is sensitive to the internuclear distance of the neighboring atoms. So far, there have been no studies that have explored how the shape resonances are influenced by modifying the shape of the molecules in the initial state, e.g. by causing non-symmetric vibrations. In this paper, where we have considered the prototypical linear triatomic molecules CO_2 and N_2O, we find that the peaks of the prominent shape resonances that occur at about 20 eV above the threshold are reduced and shifted to lower energy by excitation of the bending vibrations in the electronic ground state. An analysis of the corresponding computed results shows that these changes are due to a combination of changes in the energy of the resonant state as a function of the bending angle and of changes in lifetime of the resonant state. We also show that the total cross section for ionization from a vibrationally excited molecule is, to a good approximation, the cross section at a fixed bending angle, where the angle is given by the root mean square (rms) value of the bending normal coordinate for the initial state.

2. Experimental methods

The experiments on the core ionization of CO_2 and N_2O were carried out at beamline 27SU [10] at SPring-8 in Japan, using the high-resolution varied line-spacing plane grating soft x-ray monochromator [11]. The bandwidth was $\sim$100 meV for energies just above the C $(1s)^{-1}$ threshold for a resolving power of 3000, $\sim$85 meV just above the N $(1s)^{-1}$ threshold for a resolving power of 5000 and $\sim$110 meV just above the O $(1s)^{-1}$ threshold for a resolving power of 5000. The radiation source is a figure-8 undulator that can provide soft x-rays with either horizontal or vertical linear polarization by setting the undulator gap appropriately [12, 13]. Two identical ion detectors with retarding potentials of +6 V were orientated at 0° and 90° with respect to the E vector of the horizontally polarized incident light [14, 15]. The acceptance angle for the fragment ions was about $\pm 9°$. The ratio of the detection efficiencies of the two detectors was determined by comparing angle-resolved ion yield (ARIY) spectra recorded using horizontally and vertically linearly polarized light. The high-temperature sample gas was produced using a resistively heated molecular beam source. The ARIY spectra were recorded at source temperatures of 300 and 700 K. The temperature of the gas target was modified by heating the wall of a metal pipe of about 30 cm in length through which target gas was fed. Care was taken to confine thermal radiation emitted by the heater using a water-cooled jacket, which surrounded the metal pipe and the heater. The temperature of the nozzle was monitored with a thermocouple. To compensate for changes in density in the source volume (due to the temperature differences) the angle-resolved spectra are normalized to the areas of the combined spectra $I(54.7°) = I(0°) + 2 \times I(90°)$ over the whole energy range at both 300 and 700 K [7, 8].

The vibrational population distribution of the sample molecules at a given temperature can be estimated using the Boltzmann distribution. Assuming the Boltzmann distribution, we

estimate the population of the vibrational ground state of CO_2 (N_2O) to be 91.8% (88.3%) at 300 K and 53.2% (47.8%) at 700 K. Initial-state-specific ARIY spectra, one for the vibrational ground state and one for all vibrational excited states, can be extracted as linear combinations of the ARIY spectra recorded at 300 and 700 K. Note that at 700 K the population of the first excited state of CO_2 (N_2O) is estimated to be 26.9% (28.5%), with a further 19.9% (23.8%) of the population in higher excited states. Thus, the vibrational excited ARIY spectrum is due to ionization of molecules with one or more quanta of bending vibration excitation. Based on these assumptions, two *pure* ARIY spectra for the vibrational ground and excited states were extracted from the ARIY spectra recorded at 300 and 700 K, for each of two detection angles of 0° and 90°. Although it is difficult to estimate precisely the expected uncertainty in the reported experimental relative cross sections, our best estimate is that the uncertainties are of the order of 20–30%.

3. Theoretical methods

To interpret the experimental ARIY data, the corresponding theoretical polarization specific photoionization cross sections were computed. The approach we have taken is to use the adiabatic approximation [16] so that the fixed-nuclei cross sections for 1*s* ionization of both CO_2 and N_2O were obtained at a series of bent geometries. The sampled values of ∠OCO and ∠NNO were 180°, 172°, 164° and 156°. In all calculations the bond lengths were fixed to be the experimental equilibrium values [17], with R(C-O) = 1.15996 Å in CO_2 and with R(N-N) = 1.1273 Å and R(N-O) = 1.1851 Å in N_2O.

At each geometry, the cross section was computed using the single-channel static-exchange correlation-polarization model [18]–[20]. In a purely static exchange calculation, the electronic wave function of the target is represented by a Hartree–Fock (HF)-type single-configuration state function so that the interaction of the photoelectron with the target electrons is reduced to a sum of one-electron operators, which are the usual Coulomb and exchange operators of HF theory [21]. In the static-exchange approximation all effects are ignored that result from the dynamic response of the electrons in the target to the motion of the continuum photoelectron. In the present study, we have approximately included the correlation missing in the static-exchange approximation by including a local density functional-type correlation potential [18]. This approach has been used with some success previously both in electron–molecule scattering studies and in calculations of molecular photoionization cross sections [22]. We note that including such correlation effects is particular important for obtaining reasonable estimates of the position of low-energy scattering resonances, such as those found in the present study.

In HF-like calculations for core ionization processes, such as those performed here, the positions of low-energy resonances are sensitive to the actual orbitals used to represent the bound electrons. At one extreme, one can perform a frozen-core HF (FCHF) calculation where the orbitals in the ion are taken to be the same HF orbitals as in the unionized initial state. At the other extreme, one can use relaxed orbitals, where the orbitals are obtained from an HF calculation on the ion state where there is a hole present in the appropriate core orbital. This relaxed-core HF (RCHF) approach includes the effects of contraction of the molecular orbitals that occurs during the ionization process. Empirically, it has been observed that calculations using the frozen core approach tend to have resonances at energies below the experimental result, whereas the relaxed core tends to lead to resonances at too high an energy [23, 24]. The RCHF approach has also been modified to use a fractional charge on the core holes

leading to the RCHF with fractional charge (RCHFFC) method [25]. Here we have instead used orbitals obtained within the equivalent core approximation (ECA) [26, 27]. In the ECA, the wave function of the ionic state containing the core hole is approximated by the ground state of an ion where the charge on the nucleus where the core hole is formed is increased by one. In the case of N_2O, the wave function for the molecule with a hole in the $1s$ orbital on the terminal N atom, denoted as N_t $(1s)^{-1}$, is represented by the ground state of the ONO^+ molecule. However, the calculation is performed using the bond lengths of the original N_2O molecule. Likewise, for a hole formed on the central N atom, denoted as N_c $(1s)^{-1}$, the state is represented by the ground state of the NOO^+ molecule. Finally, for the O $(1s)^{-1}$ state in N_2O^+, the NNF^+ ground state is used. In CO_2^+, the orbitals in the O $(1s)^{-1}$ state were computed from a ground state calculation on FCO^+. Likewise the orbitals for the C $(1s)^{-1}$ state were obtained using the ground state of ONO^+. It is known that the ECA can form the basis for the computation of very accurate potential energy surfaces for the core hole states [26, 27]. Here we will explore the utility of such an approximation for computing photoionization transition moments within a single-channel HF-like treatment of the scattering problem, leading to what we will refer to as equivalent-core HF (ECHF) results. In all calculations, we employed the augmented correlation-consistent-polarized valence triple-ζ (aug-cc-pVTZ) [28, 29] one-electron basis set.

4. Results and discussion

In figures 1 and 2, we compare total cross sections computed using the ECHF with other theoretical and selected experimental cross sections published previously. In figure 1, we compare the experimental data for core ionization of N_2O from Schmidbauer *et al* [30] to fixed-nuclei FCHF and RCHF calculations [30], ECHF cross sections averaged over the bending motion and at the linear geometry, fixed-nuclei time-dependent density-functional theory (TDDFT) calculations [31] and multichannel Schwinger configuration interaction (MCSCI) calculations that have been averaged over the motion of the two stretching vibrations [32]. The experimental data in figure 1 have been scaled by 0.60 compared to the data seen in figure 2 of [30] as suggested by the authors of that paper to remove the contributions from shake-up and shake-off processes. We can see that the energy of the resonance in the ECHF results is in between the FCHF and RCHF results with a peak cross section somewhat smaller than in the RCHF calculation. The MCSCI results are seen to have very good agreement with the position of the resonance found in the experiment and in the magnitude of the cross section away from the resonance. The TDDFT calculations have resonance energies that are in good agreement with the experimental data; however, the peaks in the resonant cross sections are seen to be too high. In figure 2, we show the measured single-hole cross sections for core ionization of CO_2 from [33] and compare them to FCHF and RCHF fixed-nuclei cross sections [33] and the current ECHF averaged over the bending motions and at the equilibrium geometry. Additionally, we give the RCHFFC results that were averaged over the symmetric stretch [25]. Again, as in the case of the core ionization of N_2O, the ECHF results for the shape resonance in the core ionization of CO_2 show resonance energies that fall in energy between that found in the FCHF and RCHF calculations with peak resonance magnitudes in somewhat better agreement with the experimental single-hole cross sections than what was found in the other HF-like methods. Overall we see that the ECHF method gives the position of the shape resonances and peak cross sections in the core ionization of the systems considered here as well as any of the other methods that have been used to study these systems, with the one exception of the MCSCI, which in its

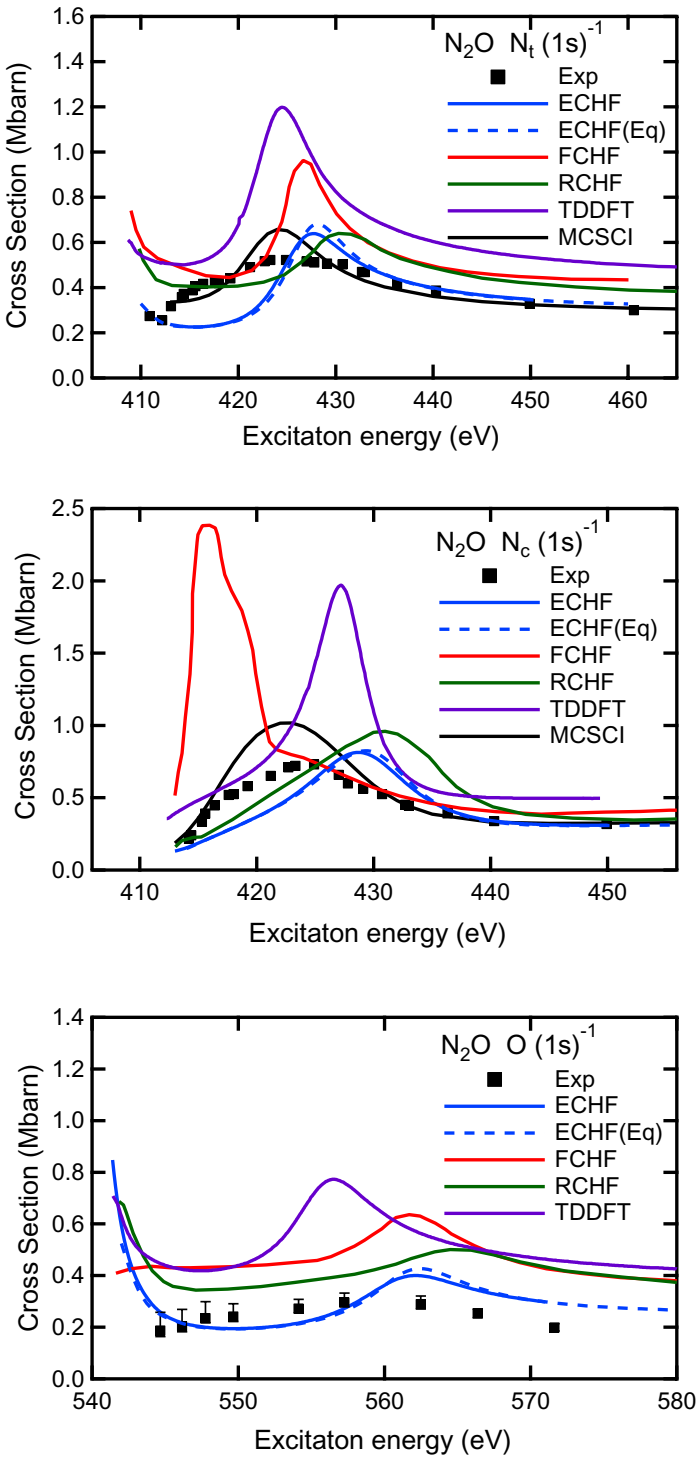

Figure 1. Comparisons of total cross sections for K-shell ionization of N_2O with previous theory and experiment. The experimental results are from [30] scaled by 0.6 to remove the shake-up and shake-off contributions. The dashed blue line gives the ECHF at the equilibrium geometry and the solid blue line is the ECHF result averaged over the bending motion of the ground state. The FCHF and RCHF data are from [30], the TDDFT data are from [31] and the MCSCI data are from [32].

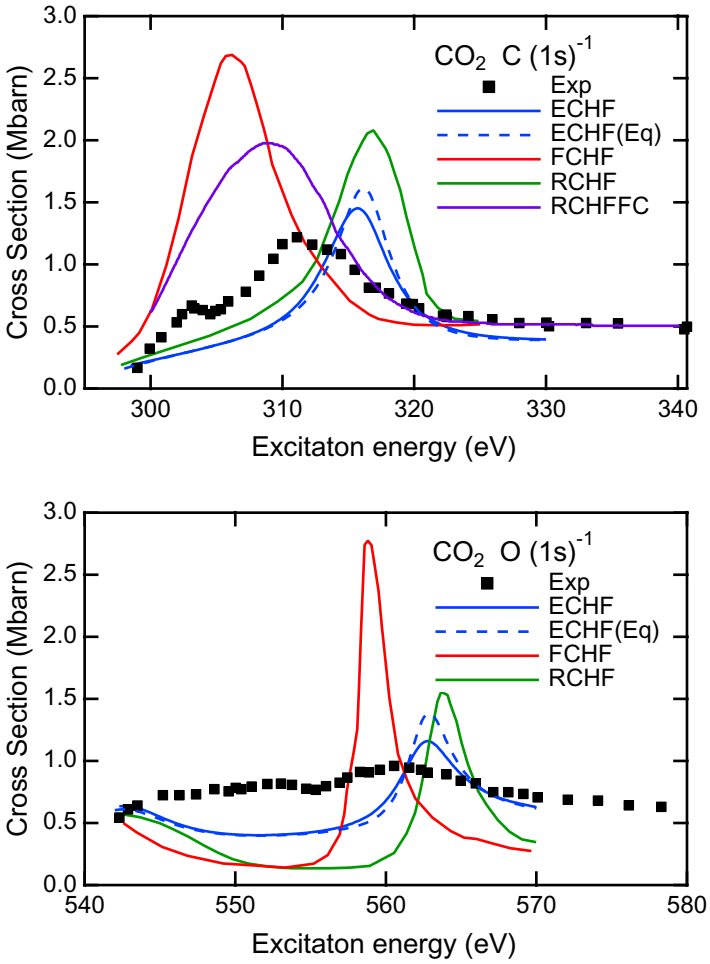

Figure 2. Comparisons of total cross sections for K-shell ionization of CO_2 with previous theory and experiment. The experimental data are the single-hole data from [33]. The dashed blue line gives the ECHF at the equilibrium geometry and the solid blue line is the ECHF result averaged over the bending motion of the ground state. The FCHF and RCHF data are from [33] and the RCHFFC results are from [25].

current implementation can only treat linear systems so that it could not be used in the present study of the effects of bending.

Polarization-specific fixed-nuclei cross sections, obtained using the method described above, for the N_t $(1s)^{-1}$, N_c $(1s)^{-1}$ and O $(1s)^{-1}$ ionization of N_2O are shown in figure 3. The fixed-nuclei cross sections for the C $(1s)^{-1}$ and O $(1s)^{-1}$ ionization of the CO_2 system are shown in figure 4. The dependence of the cross sections on the bending angle seen in these resonances is very similar to that found in the valence ionization of CO_2 as seen by Yu *et al* [34]. As noted by those authors, the position of the resonance initially does not change much with bending angle and then shifts somewhat to lower energy with increasing bending angle. One consequence of using the ECA to compute the electron–molecule interaction potential is that the ECA state used for the C $(1s)^{-1}$ state of CO_2^+ is nearly the same as that used for the $N_t(1s)^{-1}$ state of N_2O^+, except for the slight differences due to the differing bond lengths used. This similarity is reflected in the computed fixed-nuclei cross sections shown in figures 3 and 4.

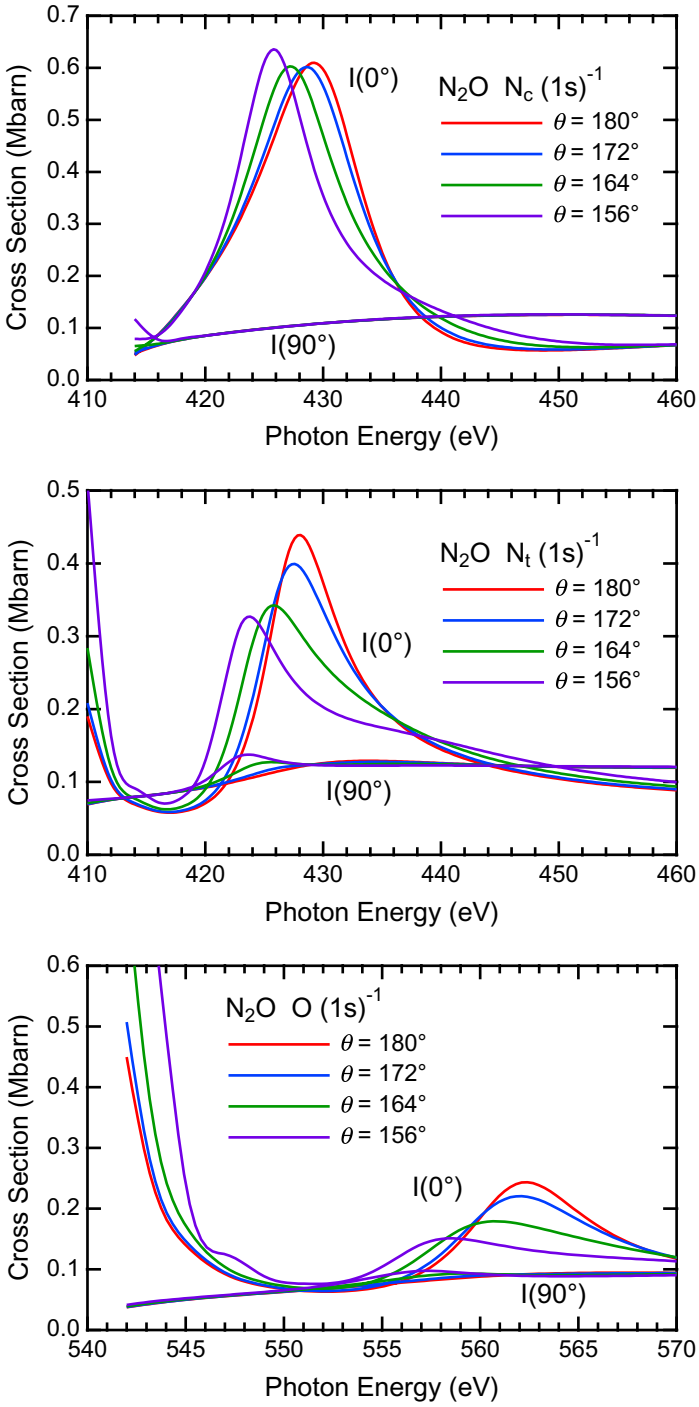

Figure 3. Computed partial cross sections for the N_t $(1s)^{-1}$, N_c $(1s)^{-1}$, and O $(1s)^{-1}$ photoionization of N_2O as a function of the bending angle.

A more quantitative analysis of the geometry dependence of the resonances can be obtained by fitting the profile of each fixed nuclei cross section using a Fano analysis [35]

$$\sigma_{\text{Total}}(E) = \sigma_0 \frac{(q+\epsilon)^2}{1+\epsilon^2} + \sigma_{\text{BG}}(E), \tag{1}$$

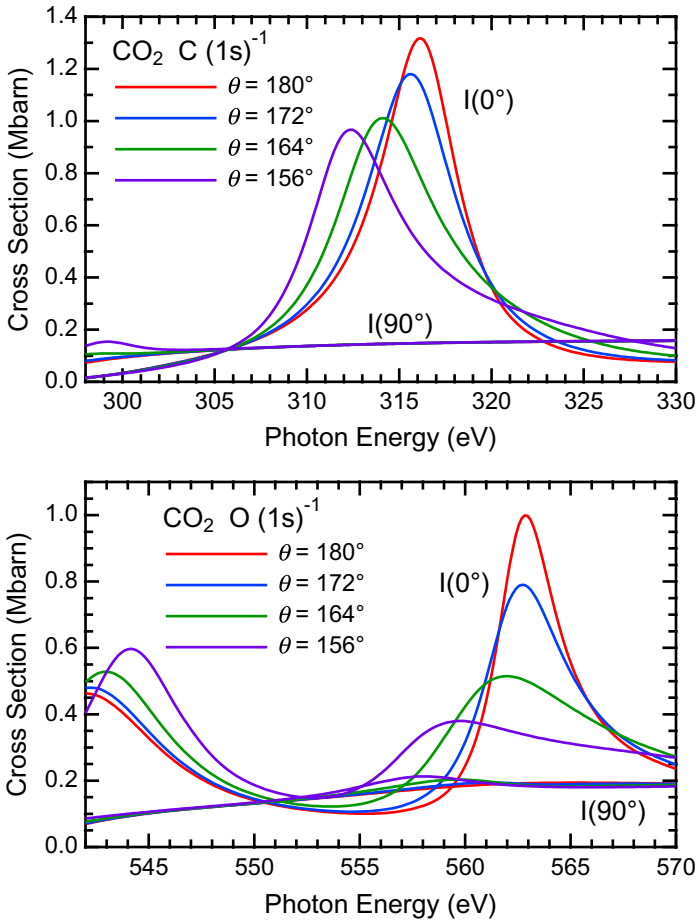

Figure 4. Computed partial cross sections for the C $(1s)^{-1}$ and O $(1s)^{-1}$ photoionization of CO_2 as a function of bending angle.

where ϵ is given by $2(E - E_R)/\Gamma$ and where E_R is the energy of the resonance that has been shifted by the interaction with the continuum and Γ is the width of the resonance. In our fits, the background cross section $\sigma_{BG}(E)$ is written as a power series in $E - E_R$ using terms up to third order. The resulting energies and widths for the various resonances are give in table 1.

We also studied the nature of the resonant states by computing the corresponding Siegert states with a cutoff potential [36]. The Siegert state is a scattering state computed at the complex energy $E_R - i\Gamma/2$, which is the location of the pole in the S matrix in the complex energy plane that is the source of the resonant behavior. Thus the wave function of the Siegert state can be used to understand the qualitative nature of the resonance, e.g. the spatial location of the resonance in the molecule and its angular momentum and nodal properties. To perform these calculations, we use the somewhat simpler local adiabatic static model-exchange (ASME) potential that we have found to be useful for obtaining a qualitative understanding of the nature of shape resonant states [20, 37, 38], such as those found in the systems considered here. In figure 5 we give the wave functions of the resonant states in the N_t $(1s)^{-1}$ continuum as a function of the bending angle. In this system, we see that the resonant state can be characterized as an antibonding valence σ_u^* resonance, where the indicated *ungerade* symmetry is only approximate in the N_2O case but is an exact symmetry in the case of C $(1s)^{-1}$ ionization of

Table 1. Position and width of resonant states in the fixed nuclei calculations.

Hole state	Angle	E_R (eV)	Γ (eV)
N_2O^+ O $(1s)^{-1}$	180°	561.6	7.38
	172°	561.0	8.32
	164°	558.2	9.94
	156°	555.7	6.98
N_2O^+ N_c $(1s)^{-1}$	180°	430.2	11.20
	172°	429.4	11.39
	164°	427.0	10.62
	156°	425.2	8.04
N_2O^+ N_t $(1s)^{-1}$	180°	427.0	7.32
	172°	426.3	8.01
	164°	423.8	7.97
	156°	422.4	5.76
CO_2^+ C $(1s)^{-1}$	180°	316.1	5.24
	172°	315.6	6.02
	164°	314.2	6.66
	156°	312.4	6.07
CO_2^+ O $(1s)^{-1}$	180°	562.9	3.34
	172°	562.7	4.14
	164°	561.6	6.00
	156°	559.3	6.02

CO_2 at the linear geometry. Note that the g–u symmetry of the resonant state will also only be approximate for the O $(1s)^{-1}$ ionization of CO_2 computed here, since in this case we use a symmetry-broken wave function in the ECHF approximation. The resonances at photoelectron energies of about 20 eV in the other ionization channels are qualitatively very similar to the resonance in the N_t $(1s)^{-1}$ channel shown in figure 5.

The most prominent feature of the resonance parameters given in table 1 is that the energy of the resonances in each case becomes lower in energy as the molecule bends. Using a simple Hückel molecular orbital (HMO) model [39, 40] as applied to an AB_2 molecule, we would expect the energy of this highest valence σ_u^* resonant state to decrease as the molecule bends and that the angle-dependent term in the energy would be proportional to $\cos^2(180^\circ - \theta)$ based on the strength of the overlap between the central p_σ orbital and the p_σ orbitals located on the terminal atoms. This expected $\cos^2(180^\circ - \theta)$ dependence is seen in the resonance energies given in table 1, where in most cases the change in E_R in going from 180° to 172° is approximately one third the change in going from 172° to 164°. The exceptions to this observation are the resonance energies associated with the O $(1s)^{-1}$ ionization, for which the extraction of the resonance parameters is much less certain since in these cases the resonances are less prominent features.

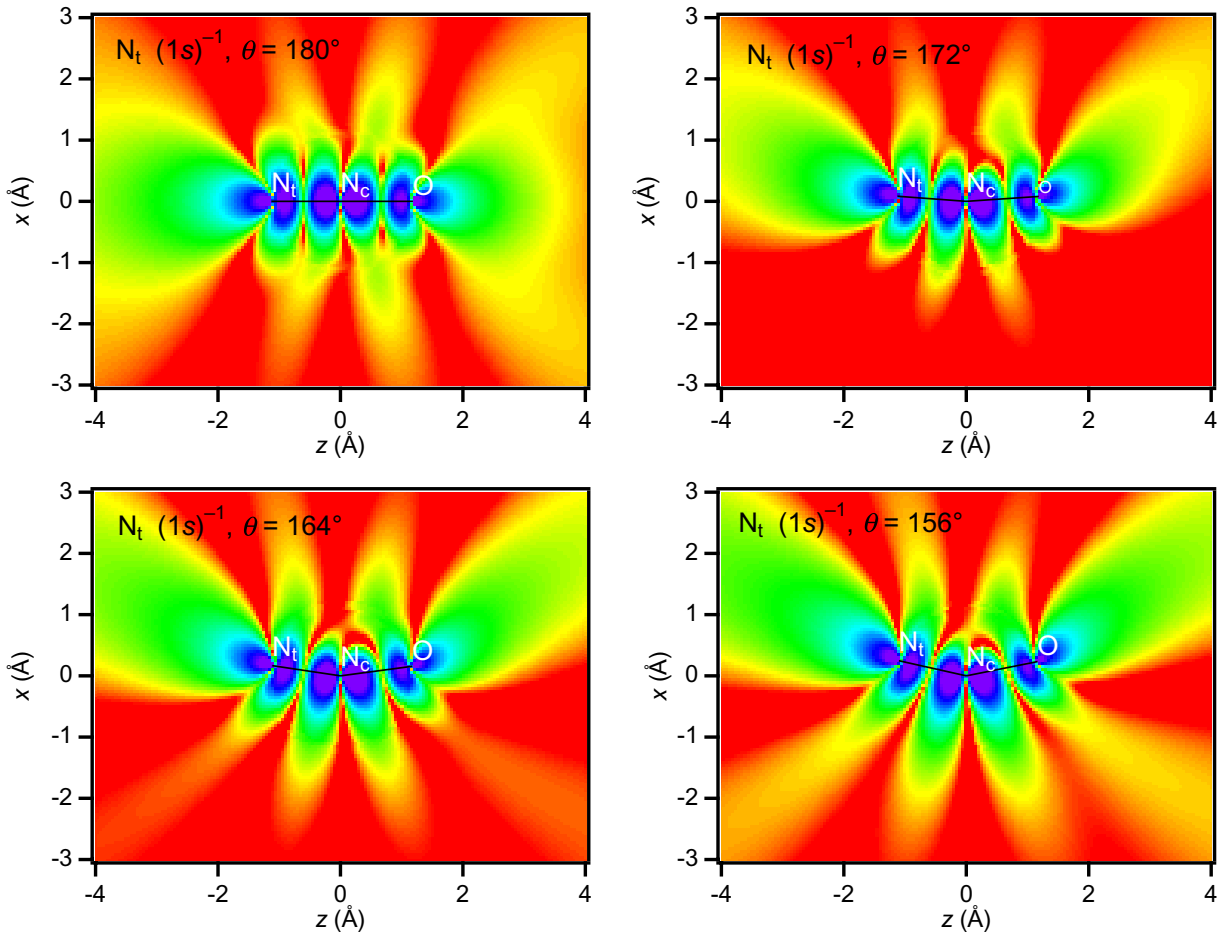

Figure 5. The probability densities of resonant Siegert states for ionization leading to the N_t $(1s)^{-1}$ of N_2O^+ as a function of bending angle.

There are two factors that control the lifetime of a shape resonant state: the energy deficit of the resonant state with respect to the dynamical angular momentum barrier and the strength of the coupling to other partial waves. In an atomic system, within a single-channel potential scattering picture, the lifetime of the resonant state is controlled by the height of the angular momentum barrier and the energy of the state relative to the top of the barrier, i.e. the energy deficit. In a one-electron diatomic system, there is a generalized angular momentum that is conserved [41, 42], leading to a factorization of the scattering wave function in confocal elliptic coordinates. In such a system, the decay of a shape resonance will then occur by tunneling through an effective angular momentum barrier. For a general linear molecule, there is only an approximate factorization, leading to the decay of resonance states by both tunneling through dynamical barriers and scattering into partial waves with lower angular momenta, which then have lower dynamical barriers leading to direct escape of the electron or much more rapid tunneling. The dependence of the widths of the resonances on bending angle for the triatomic systems considered here can be in part understood by considering the nodal structure of the resonant wave functions in figure 5 for the case of the σ_u^* resonance seen in the ionization to the N_t $(1s)^{-1}$ state of N_2O^+. We can see that in the region of the nuclei, there are five nodal surfaces

that cut across the molecular axis. This is characteristic of a state with angular momentum $l = 5$ [43]. Note, however, that in the region further away from the molecule the outgoing flux is more characteristic of an $l = 3$ partial wave, showing that there is coupling between $l = 5$ partial waves and $l = 3$ partial waves by which the electron escapes. As the molecule bends away from the linear geometry, the additional significant breaking of the g–u symmetry allows partial waves with even values of l to couple to the resonant state. In the N_t $(1s)^{-1}$ case shown in figure 5 we see the buildup of an $l = 4$ component in the wave function as the electron moves away from the molecule in the bent geometries. This coupling to additional partial waves presumably leads to shorter lifetimes of the resonant states and corresponding increased widths seen initially for most of the resonant states considered here, as given in table 1. We note, however, that all of the resonances either become narrower with further increases in the bending angle, or in the case of the CO_2^+ O $(1s)^{-1}$ state, the rate of broadening with bending angle decreases. This is probably connected to the lowering of the resonance energy with bending that will lead to larger energy deficits and slower tunneling rates. The fact that there are two competing mechanisms for the decay of shape resonances in molecular systems, with opposing effects on the widths of the resonances with changing angle, leads to the varying behavior of the resonances found in the systems considered here.

It is also of interest to note that, in addition to the σ_u^* resonance that occurs at photoelectron energies of approximately 20 eV, there is a lower-energy σ_g^* resonance that appears near the threshold in some cross sections seen in figures 3 and 4. As noted above, the high-energy resonance shown in figure 5 has approximately *ungerade* symmetry in the linear geometry. The lower-energy resonance has a corresponding approximate *gerade* symmetry. The dipole selection rule leads to the fact that this resonance is not seen in the C $(1s)^{-1}$ ionization in CO_2 but is quite prominent in the corresponding O $(1s)^{-1}$ ionization as seen in figure 4. The energy of the low-energy resonance is seen to increase with bending angle, which is in agreement with the simple HMO picture [39, 40] for this σ_g^* molecular orbital in contrast to the behavior of the σ_u^* resonances discussed above.

To see the implications of the angle-dependent resonance features for the experimental observables, we compute the vibration-state-specific cross sections from the fixed-nuclei cross sections. In the calculations, the bending vibrational wave functions were represented by harmonic oscillator functions. The frequencies used for the initial state wave functions were the experimental values [44] of 667 cm^{-1} for CO_2 and 589 cm^{-1} for N_2O. The frequencies for the ground state and the different ion states were then computed using ECA and the second-order Møller–Plesset (MP2) perturbation theory [45]. A different scaling factor was then determined for each molecule that scaled the ground state frequencies to agree with the experimental frequencies. This scaling factor was then applied to the bending potentials of the different hole states, leading to the following bending frequencies for the ion states: 569 cm^{-1} for O $(1s)^{-1}$ and 590 cm^{-1} for C $(1s)^{-1}$ in CO_2^+, 555 cm^{-1} for N_t $(1s)^{-1}$, 561 cm^{-1} for $N_c(1s)^{-1}$ and 447 cm^{-1} for O $(1s)^{-1}$ in N_2O^+. In the calculated cross sections, we have computed the vibrational-state-specific cross section for ionization from either the ground state, $(0, 0, 0)$ or the state with one quanta of excitation in the bending mode $(0, 1^1, 0)$, to all bending states of the ion with appreciable excitation probability. The form of the cross section is then [16]

$$\sigma_{v_2^+,l^+\leftarrow v_2,l} = \left| \int \int \chi_{v_2,l}(q) \frac{e^{-il\phi}}{\sqrt{2\pi}} f(q,\phi) \chi_{v_2^+,l^+}(q) \frac{e^{il^+\phi}}{\sqrt{2\pi}} q \, dq \, d\phi \right|^2, \tag{2}$$

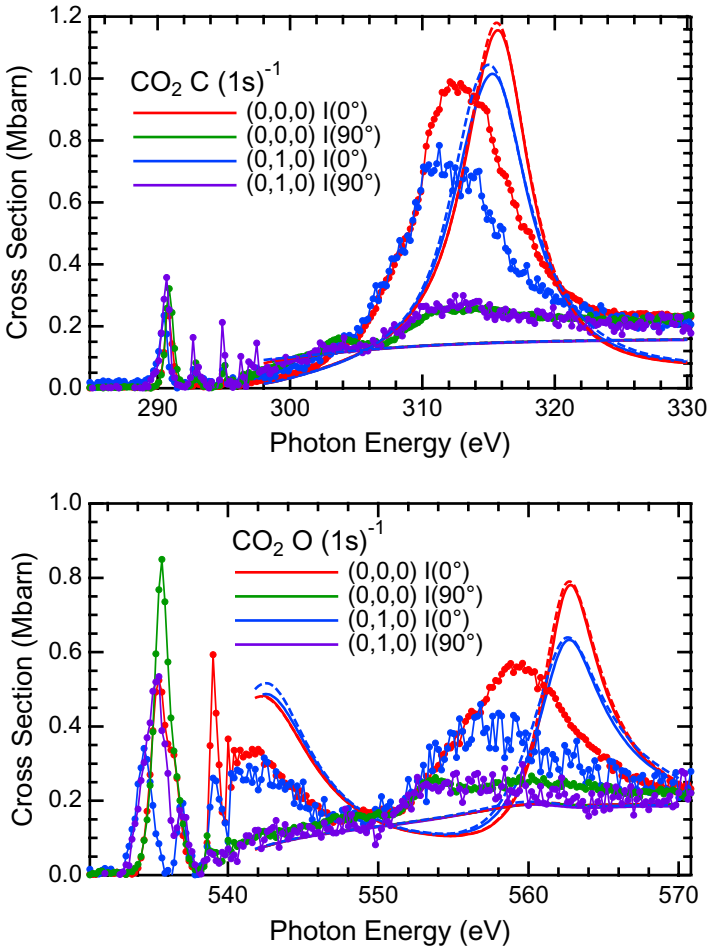

Figure 6. Experimental (connected dots) and computed (solid lines) ARIY spectra in the CO_2 C $1s^{-1}$ and O $1s^{-1}$ σ^* shape resonance regions. The dashed lines are computed using equation (6) with $q_{\nu_2,l}^{(\mathrm{rms})}$ having values corresponding to bending angles of 172.6° for the (0, 0, 0) initial state and 169.5° for the (0, 1^1, 0) state.

where $\chi_{\nu_2,l}(q)$ is the radial part of the 2D bending vibrational initial state wave function in cylindrical coordinates with vibrational quantum number ν_2 and vibrational angular momentum quantum number l, $\chi_{\nu_2^+,l^+}(q)$ is the corresponding final ionic vibrational radial wave function, q and ϕ are the bending normal coordinates where $q = 0$ corresponds to a linear geometry, and $f(q, \phi)$ is the dipole transition moment. The cross sections were then summed over the final vibrational states to obtain the total cross sections $\sigma_{\nu_2,l}$. The total cross sections and the corresponding ARIY experimental data are shown in figure 6 for CO_2 and figures 7 and 8 for N_2O.

The total cross sections can be related to fixed-nuclei cross sections at bent geometries with certain assumptions. If the difference in the photoelectron kinetic energy between the different final vibrational states is ignored, then the total cross section is [46]

$$\sigma_{\nu_2,l} = \int [\chi_{\nu_2,l}(q)]^2 \sigma(q)\, q\, \mathrm{d}q, \tag{3}$$

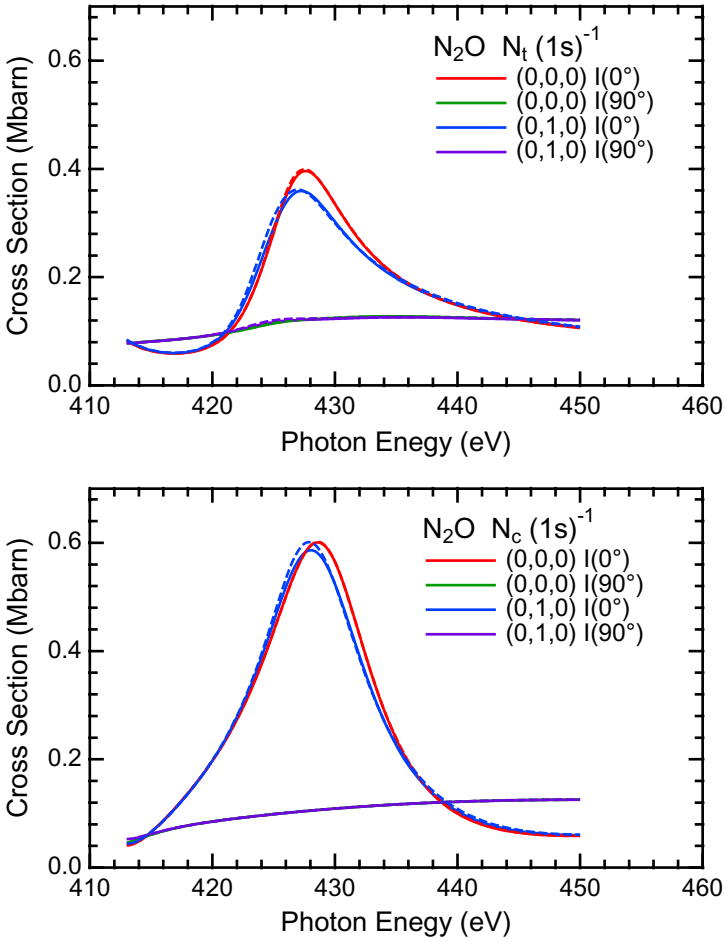

Figure 7. Computed ARIY for the K-shell photoionization of N_2O for the N_t $(1s)^{-1}$ and N_c $(1s)^{-1}$ hole states. See the caption of figure 6 for the line types. The bending angles used in equation (6) were 172.4° for the (0, 0, 0) initial state and 169.3° for the $(0, 1^1, 0)$ state.

where the fixed-nuclei cross section $\sigma(q)$ is given by

$$\sigma(q) = \frac{1}{2\pi} \int |f(q, \phi)|^2 \, \mathrm{d}\phi. \tag{4}$$

For bending modes, the dependence of the fixed-nuclei cross section on q has no first order term so that a power series expansion has the form [34]

$$\sigma(q) = \sigma^{(0)} + q^2 \sigma^{(2)} + \cdots. \tag{5}$$

Then by ignoring higher-order terms, the total cross section in equation (3) can be approximated by

$$\sigma_{\nu_2,l} \approx \sigma^{(0)} + \left(q_{\nu_2,l}^{(\mathrm{rms})}\right)^2 \sigma^{(2)} \approx \sigma\left(q_{\nu_2,l}^{(\mathrm{rms})}\right), \tag{6}$$

where the rms value of the normal coordinate q is given by

$$q_{\nu_2,l}^{(\mathrm{rms})} = \left[\int \chi_{\nu_2,l}^2(q)\, q^3 \, \mathrm{d}q\right]^{1/2}. \tag{7}$$

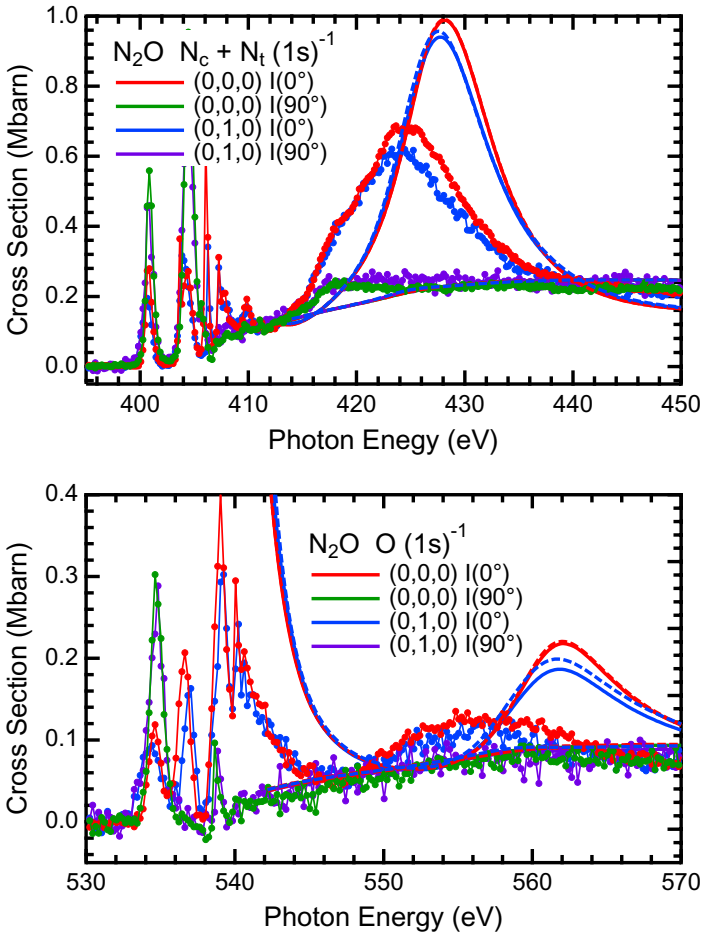

Figure 8. Comparison of measured and computed ARIY for the K-shell photoionization of N_2O. See the caption of figure 6 for the line types. The bending angles used in equation (6) were 172.4° for the $(0, 0, 0)$ initial state and 169.3° for the $(0, 1^1, 0)$ state.

Thus the total cross sections for ionization for different initial bending states are a direct measure of the fixed-nuclei cross sections at the bent geometry corresponding to $q_{\nu_2,l}^{(\mathrm{rms})}$. This analysis is very similar to that performed for the effects of final state stretching on shape resonances by Mistrov *et al* [47].

The ARIY data shown in figures 6 and 8 are not absolute and have been scaled so that experiment and theory have similar values. The energy scale for the calculations was fixed by using the experimental ionization potentials for the various hole states. In the C $(1s)^{-1}$ data for the ionization of CO_2 given in figure 6, the peak in the computed shape resonance feature in the 0° cross section occurs at an energy of ∼4 eV above the experimental results as was seen in the comparison of the total computed and measured cross sections given in figure 2. However, the width of the peaks and the size of the change in the computed cross sections due to the vibrational excitation of the initial state correspond quite well to those seen in the measured data.

The corresponding data for the core ionization of N_2O are given in figures 7 and 8. We note that in the experiment the photoelectron is not detected so that at a given photon energy the

experimental ARIY intensity is a sum over the contributions from all open ionization channels. In particular, the contributions from the N_t and N_c ionization channels are combined in the experimental data, and given that the shape resonances in these two channels occur at nearly the same photon energy as seen in figure 7, there appears only a single shape resonant feature as seen in figure 8. Although the experimental data for the O $(1s)^{-1}$ ionization are noisier, one also sees a change in intensity in the region of the resonance near 558 eV that is similar to the computed change seen in the lower panel of figure 8.

In figures 6–8, we have also plotted the total vibrational-state-specific cross sections obtained using equation (6). One can see that equation (6) is very accurate for the cross section for ionization from the (0, 0, 0) states and is still a very good approximation for ionization from the $(0, 1^1, 0)$ states. Thus, we can expect that the corresponding experimental vibrational-state-specific cross sections should be a direct measure of the total fixed-nuclei cross sections at the corresponding $q_{\nu_2,l}^{(\mathrm{rms})}$ geometries.

We note that the behavior of the σ_u^* resonance in the N_c $(1s)^{-1}$ channel of N_2O ionization, as seen in figure 7, is different from the other cases considered. In figure 3, we see that the intensity of the resonance in this case actually increases with increased bending in contrast to the other cases considered. This increase in peak cross section with bending angle can be attributed to the fact that the resonance width in this channel increases very little before beginning to decrease with increasing bending angle as seen in table 1. This difference in behavior in the theory is seen in vibrationally specific cross sections in figure 7 where the N_c $(1s)^{-1}$ cross section is nearly the same in the ground and excited states with only a slight shift to lower energy. The effects of the unusual behavior in the N_c $(1s)^{-1}$ ionization can also be seen in the summed cross sections for the N_c $(1s)^{-1}$ and $N_t(1s)^{-1}$ ionization shown in figure 8, where there is reduced attenuation of the cross section in both the measured ARIY and computed photoionization cross sections, compared to the other channels considered here.

5. Conclusions

In summary, we measured the ARIY for the ground and vibrationally excited CO_2 and N_2O molecules in the region of the shape resonances above the K-shell thresholds. Experimentally, the resonances at about 20 eV above the threshold are seen to have a reduced peak cross section when ionization occurs from the excited vibrational state and resonances energies are seen to shift to slightly lower energy. We have explained these observations using a 1D adiabatic ECHF model. Within this model we see that there is a shape resonance that can be described as a valence σ_u^* state. This state shifts to lower energy in the model with bending and in most channels the peak in the cross section is reduced with bending. The resulting vibrationally averaged cross sections are in reasonable agreement with the experimental data supporting the conclusion that the adiabatic ECHF model can be used to explain the experimental observations. We have then explored the behavior of the adiabatic ECHF model in terms of much simpler qualitative models. These considerations lead us to the conclusion that the shifts in the resonance energies with bending angle can be understood using the HMO model. We note that the HMO model also correctly describes the behavior of the resonance energy of the σ_g^* resonance which occurs at the threshold in some of the ionization channels considered here. The behavior of the resonance widths with bending angle could be qualitatively understood by a consideration of the mechanisms for the decay of shape resonances in molecules, including the scattering to additional partial waves with bending and the changes in the energy deficit relative to the height

of the effective angular momentum barrier. Finally, we have also shown that the cross sections for excitation from different vibrational bending states can be approximated by fixed-nuclei cross sections at specific bending angles given by the rms of the bending displacement variable.

Acknowledgments

The experiment was carried out with the approval of JASRI and supported in part by Grants-in-Aid for Scientific Research from the Japan Society for the Promotion of Science (JSPS). RRL acknowledges support from the Office of Basic Energy Sciences, the US Department of Energy and from the Robert A Welch Foundation (Houston, TX, USA) under grant number A-1020. This work was also supported by the Texas A&M University Supercomputing Facility.

References

[1] Dehmer J L 1984 *Resonances in Electron–Molecule Scattering, van der Waals Complexes, and Reactive Chemical Dynamics* ed D G Truhlar (Washington, DC: American Chemical Society) pp 139–63
[2] Piancastelli M N 1999 *J. Electron Spectrosc. Relat. Phenom.* **100** 167–90
[3] Lucchese R R, Bozek J D, Das A and Poliakoff E D 2009 *J. Chem. Phys.* **131** 044311
[4] Wu C Y R, Judge D L and Matsui T 2005 *J. Electron Spectrosc. Relat. Phenom.* **144–7** 123–6
[5] Ferch J, Masche C, Raith W and Wiemann L 1989 *Phys. Rev.* A **40** 5407–10
[6] Kato H, Kawahara H, Hoshino M, Tanaka H, Campbell L and Brunger M J 2008 *Chem. Phys. Lett.* **465** 31–5
[7] Tanaka T, Makochekanwa C, Tanaka H, Kitajima M, Hoshino M, Tamenori Y, Kukk E, Liu X J, Prümper G and Ueda K 2005 *Phys. Rev. Lett.* **95** 203002
[8] Tanaka T *et al* 2006 *Chem. Phys. Lett.* **428** 34–8
[9] Tanaka T *et al* 2008 *Phys. Rev.* A **77** 012709
[10] Ohashi H, Ishiguro E, Tamenori Y, Kishimoto H, Tanaka M, Irie M, Tanaka T and Ishikawa T 2001 *Nucl. Instrum. Methods* A **467–8** 529–32
[11] Ohashi H *et al* 2001 *Nucl. Instrum. Methods* A **467–468** 533–6
[12] Tanaka T and Kitamura H 1995 *Nucl. Instrum. Methods* A **364** 368–73
[13] Tanaka T and Kitamura H 1996 *J. Synchrotron Radiat.* **3** 47–53
[14] Kiyoshi U 2003 *J. Phys. B: At. Mol. Opt. Phys.* **36** R1–R47
[15] Saito N *et al* 2000 *Phys. Rev.* A **62** 042503
[16] Miller J S, Poliakoff E D, Miller T F III, Natalense A P P and Lucchese R R 2001 *J. Chem. Phys.* **114** 4496–504
[17] Kuchitsu K (ed) 1998 *Structure of Free Polyatomic Molecules: Basic Data* (Berlin: Springer)
[18] Perdew J P and Zunger A 1981 *Phys. Rev.* B **23** 5048–79
[19] Gianturco F A, Lucchese R R and Sanna N 1994 *J. Chem. Phys.* **100** 6464–71
[20] Natalense A P P and Lucchese R R 1999 *J. Chem. Phys.* **111** 5344–8
[21] Lane N F 1980 *Rev. Mod. Phys.* **52** 29–119
[22] dos Santos A S, Machado L E, Lee M-T, Brescansin L M and Lucchese R R 2009 *Chem. Phys.* **358** 96–102
[23] Lynch D L and McKoy V 1984 *Phys. Rev.* A **30** 1561–4
[24] Schirmer J, Braunstein M and McKoy V 1990 *Phys. Rev.* A **41** 283–300
[25] Hoshino M, Nakagawa K, Tanaka T, Kitajima M, Tanaka H, De Fanis A, Wang K, Zimmermann B, McKoy V and Ueda K 2006 *J. Phys. B: At. Mol. Opt. Phys.* **39** 3047–56
[26] Thomas T D, Saethre L J, Sorensen S L and Svensson S 1998 *J. Chem. Phys.* **109** 1041–51
[27] Dobrodey N V, Koppel H and Cederbaum L S 1999 *Phys. Rev.* A **60** 1988–2001
[28] Dunning T H Jr 1989 *J. Chem. Phys.* **90** 1007–23
[29] Kendall R A and Dunning T H Jr 1992 *J. Chem. Phys.* **96** 6796–806

[30] Schmidbauer M, Kilcoyne L D, Randall K J, Feldhaus J, Bradshaw A M, Braunstein M and McKoy V 1991 *J. Chem. Phys.* **94** 5299–305
[31] Adachi J, Ito K, Yoshii H, Yamazaki M, Yagishita A, Stener M and Decleva P 2007 *J. Phys. B: At. Mol. Opt. Phys.* **40** 29–47
[32] Lucchese R R, Soderstrom J, Tanaka T, Hoshino M, Kitajima M, Tanaka H, De Fanis A, Rubensson J E and Ueda K 2007 *Phys. Rev.* A **76** 012506
[33] Schmidbauer M, Kilcoyne A L D, Köppe H M, Feldhaus J and Bradshaw A M 1995 *Phys. Rev.* A **52** 2095–108
[34] Yu C-H, Pitzer R M and McCurdy C W 1988 *J. Phys. Chem.* **92** 3116–22
[35] Fano U 1961 *Phys. Rev.* **124** 1866–78
[36] Tolstikhin O I, Ostrovsky V N and Nakamura H 1998 *Phys. Rev.* A **58** 2077–96
[37] Lucchese R R and Gianturco F A 1996 *Int. Rev. Phys. Chem.* **15** 429–66
[38] Gianturco F A and Lucchese R R 1999 *J. Chem. Phys.* **111** 6769–86
[39] Gavin R M Jr 1969 *J. Chem. Educ.* **46** 413–22
[40] Burdett J K 1980 *Molecular Shapes: Theoretical Models of Inorganic Stereochemistry* (New York: Wiley)
[41] Erikson H A and Hill E L 1949 *Phys. Rev.* **75** 29–31
[42] Coulson C A and Joseph A 1967 *Int. J. Quantum Chem.* **1** 337–47
[43] Poliakoff E D and Lucchese R R 2006 *Phys. Scr.* **74** C71–9
[44] Herzberg G 1966 *Molecular Spectra and Molecular Structure. III. Electronic Spectra and Electronic Structure of Polyatomic Molecules* (New York: Van Nostrand-Reinhold)
[45] Frisch M J *et al* 2004 *GAUSSIAN03* (Wallingford, CT: Gaussian)
[46] Raseev G, Le Rouzo H and Lefebvre-Brion H 1980 *J. Chem. Phys.* **72** 5701–9
[47] Mistrov D A, De Fanis A, Kitajima M, Hoshino M, Shindo H, Tanaka T, Tamenori Y, Tanaka H, Pavlychev A A and Ueda K 2003 *Phys. Rev.* A **68** 022508